Chapter 4

Results and Discussions

This chapter presents the experimental results in the present work and the theoretical predictions previously reported. Physical properties, i.e., SEM profiles of the connectivity, density, heat capacity are the first described and then the electromechanical effect, i.e., the piezoelectricity, the electrothermal effect pyroelectricity and the related phenomenon " thermal diffusivity" are reported.

The SEM micrographs of the composites of 0-3 connectivity are shown in Figure 4.1. From the figure 4.1, the PZT clusters have an average particle size of about 1 μm and uniform dispersion in the copolymer matrix. Figure 4.2 shows the SEM micrograph of the composite with 1-3 connectivity. The separation of the ceramic rods are clearly seen. The density and heat capacity of the composites correspond to the volumetric averages as listed in Table 4.1. Heat flow plotted as a function of the temperature of the composites are shown in appendix C.

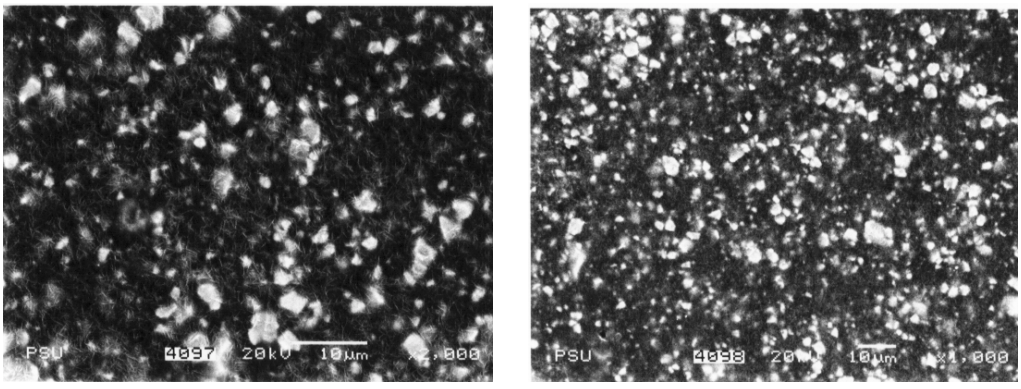

(A) (B)

Figure 4.1 Scanning electron micrographs of the 0-3 composite PZT/P(VDF-TrFE) ($\phi = 0.3$) A) $\times 2,000$ B) $\times 1,000$

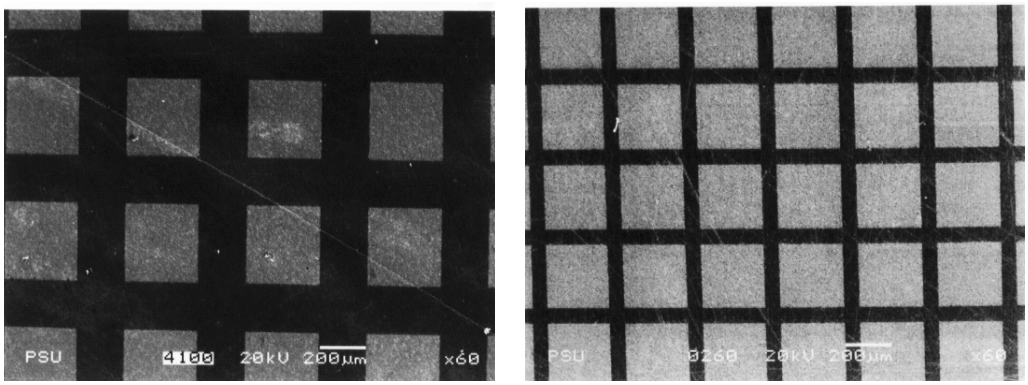

(A) B)

Figure 4.2 Scanning electron micrograph of the 1-3 composite PZT/epoxy A) ϕ = 0.4 B) ϕ= 0.6

Table 4.1 Values of the density, heat capacity and dielectric constant of the composites

Materials	ϕ	ρ $.\times 10^3\, kg/m^3.$	c_p $(J/kg\ ^oC)$	ε (F/m)
1-3 composite PZT/epoxy	0	1.1	2777*	2
	0.4	3.7	214*	500
	0.6	5.0	283*	800
	1	7.7	420	1900
0-3 composite PZT/P(VDF-TrFE)	0.3	1.88	2753*	-

*see Appendix C

1. Evaluation of the piezoelectric coefficient

Figure 4.3 shows the piezoelectric response of the poled PZT at a frequency of 1 *kHz*. The responses show a linear relation between the displacement and driving voltage. The piezoelectric coefficient d_{33} of the PZT was obtained from the slope of this plot. Figure 4.4 shows the piezoelectric response of the poled PZT in a frequency range from 1 *kHz* to 5 *kHz*. The value of d_{33} of the PZT, obtained in frequency range from 1 *kHz* to 5 *kHz*, was 360± 10 *pm/V*.

The piezoelectric response of 1-3 composite both volume fraction of ceramic 0.6 and 0.4 were obtained. Variation of displacement with driving voltage of these composites are shown in Figure 4.5 to Figure 4.8.

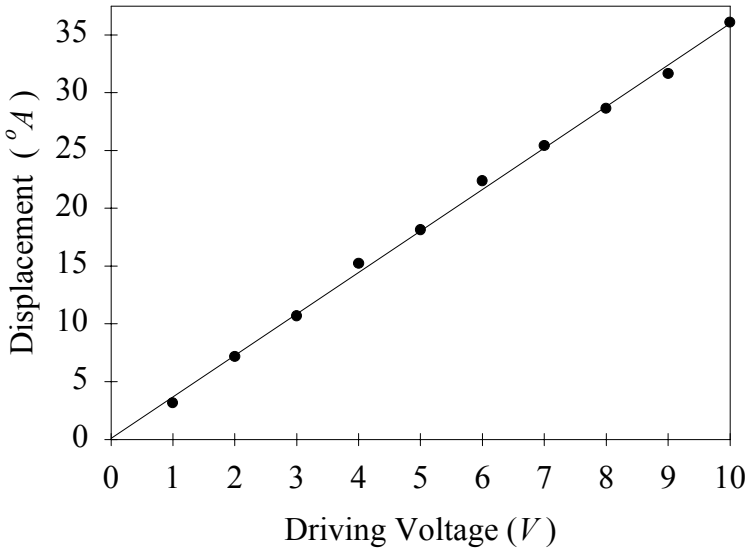

Figure 4.3 Surface displacement versus driving voltage of the poled PZT (□ = 1) at 1 *kHz*.

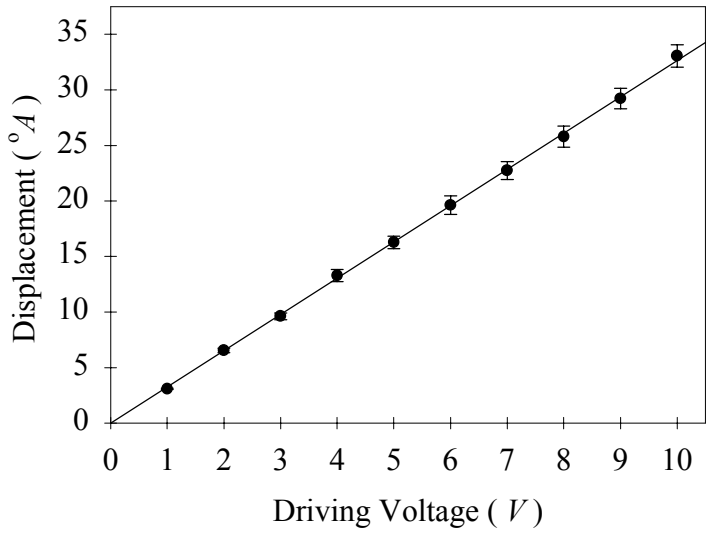

Figure 4.4 Surface displacement of the poled PZT (ϕ = 1) plotted as a function of driving voltage averaged over the frequency range of 1 *kHz* to 5 *kHz*.

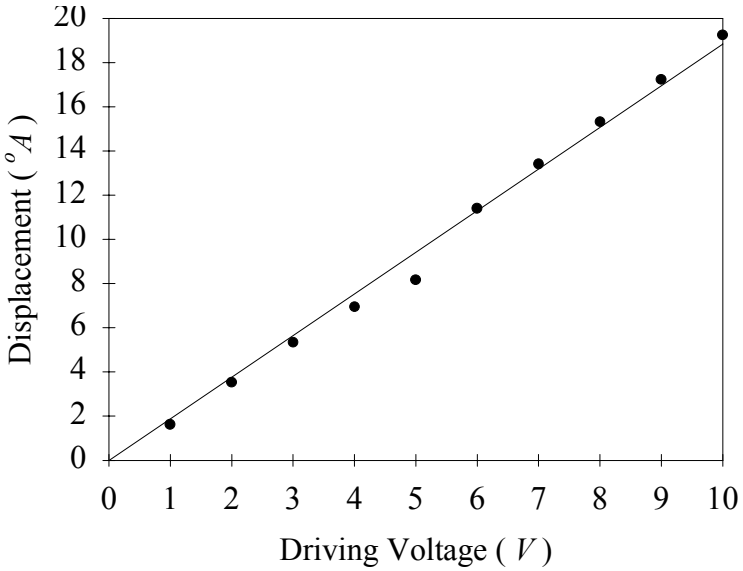

Figure 4.5 Surface displacement versus driving voltage of the 1-3 composite PZT/epoxy (ϕ = 0.6) at 1 *kHz*.

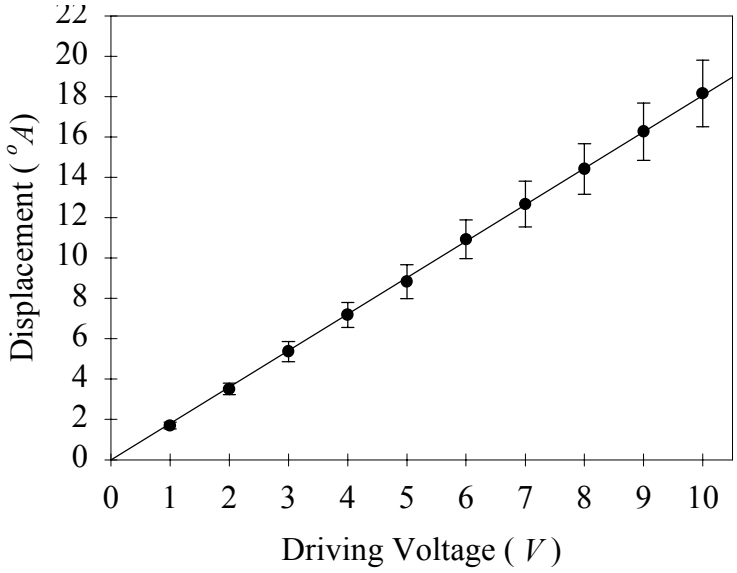

Figure 4.6 Surface displacement of the 1-3 composite PZT/epoxy ($\phi = 0.6$) plotted as a function of driving voltage averaged over the frequency range of 1-5 *kHz*.

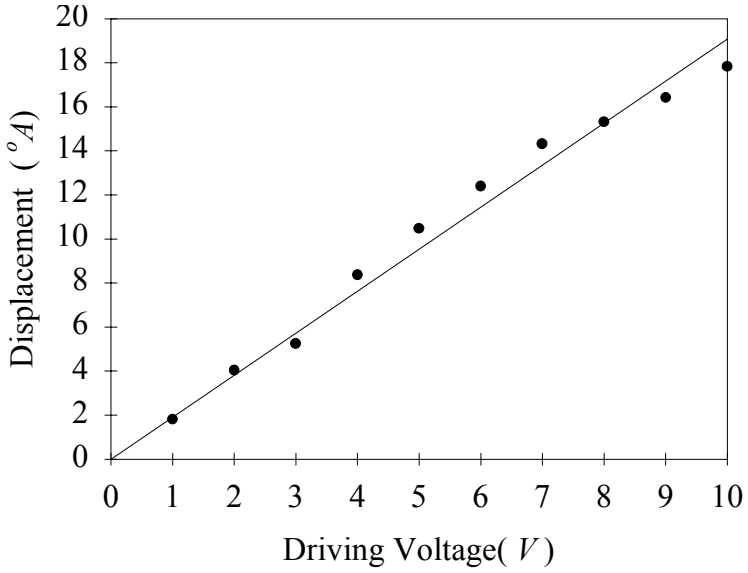

Figure 4.7 Surface displacement versus driving voltage of the 1-3 composite PZT/epoxy ($\phi = 0.4$) at 1 *kHz*.

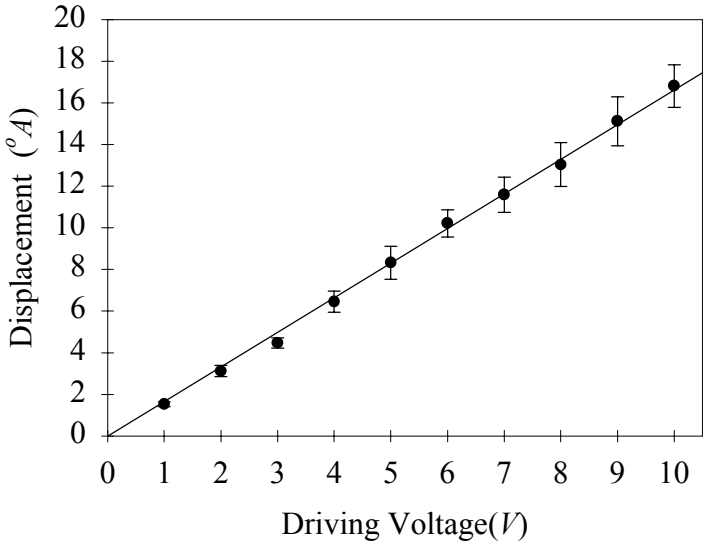

Figure 4.8 Surface displacement of the 1-3 composite PZT/epoxy (□ = 0.4) plotted as a function of driving voltage averaged over the frequency range of 1-5 *kHz*.

From Figure 4.4 to Figure 4.8, it is apparent that the piezoelectric responses of the composites both 0.4 and 0.6 volume fraction of PZT shown a linear relation between the displacement and driving voltage. The measured d_{33} coefficient of the composites having 0.4 and 0.6 volume fraction of PZT were 190 ± 10 and 188 ± 10 pm/V, respectively. These values were measured in a frequency range, which was lower than that of the PZT in order to avoid problems of the heat generated in the composites when they were driven under a high AC field. Figure 4.9 shows the value of d_{33} for the frequency range from 1-9 kHz of the poled PZT and the composites. Using equation (2.14), the value of g_{33} was found to be 43×10^{-3}, 27×10^{-3} and 22 $\times10^{-3}\, m^2/C$ for the composites having 0.4 and 0.6 volume fraction of PZT and poled PZT, respectively.

As discussed by Chan and Unsworth, the d_{33} value of the composite will be higher than that predicted from a volumetric average because the elastic compliance of the polymer is higher than that of the PZT. Figure 4.10 shows the theoretical predictions of the d_{33} values for the composites. The d_{33} values of the composites in

this work agreed closely with this prediction, however, were about 50% of that of the PZT. This may be related to incomplete poling of the PZT or heat accumulated in the epoxy.

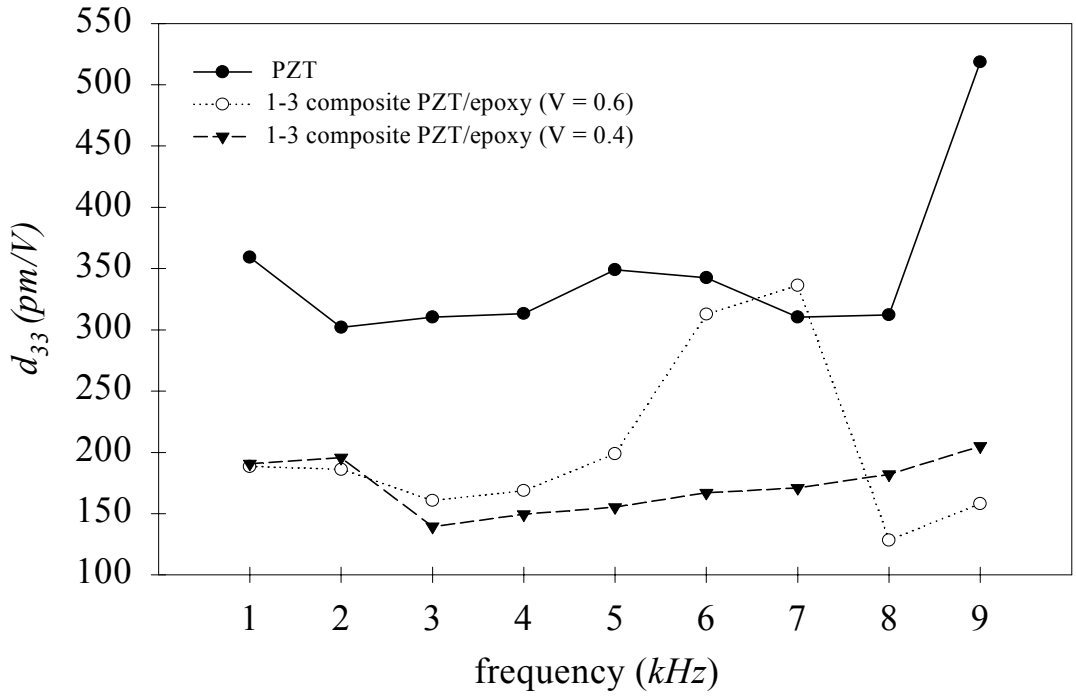

Figure 4.9 Plot of the frequency dependence of measured d_{33} of PZT and composite

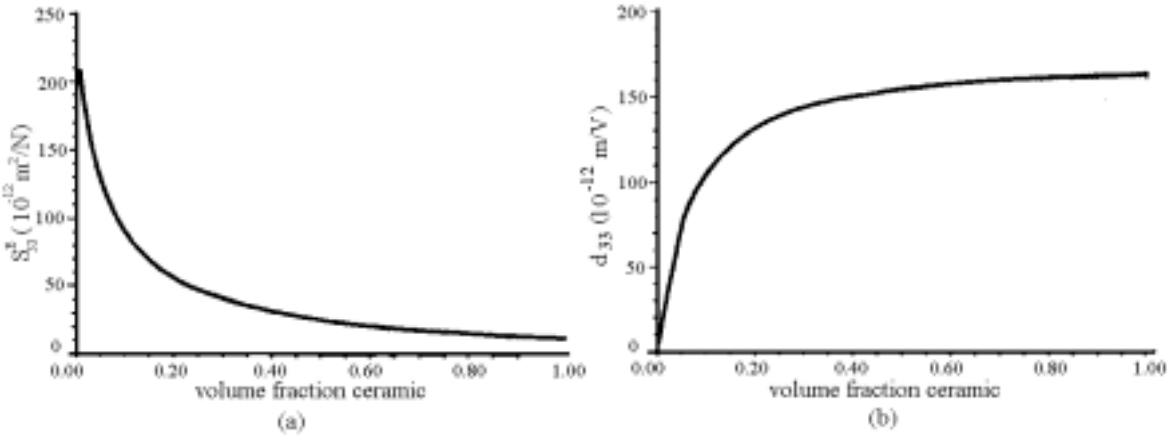

Figure 4.10 Theoretical predicted values of a) elastic compliance (S_{33}^{E}) b) piezoelectric coefficient (d_{33}) for the 1-3 composites PZT/epoxy (Chan and Unsworth, 1989)

2. Evaluation of the pyroelectric coefficient

Figure 4.11 shows a typical temperature variations in the pyroelectric coefficient measurements. It is seen that the increase of the magnitude of the current passing through the peltier element produces an increase in the temperature variation. To ensure uniform temperature distributions in the sample, 1 ampere of the current was applied to the peltier element to vary the temperature lowly.

In order to check the performance of the system, measurements were made on the $LiNbO_3$. The variation of the polarization plotted as a function of the temperature was obtained. The slope of the plot is the pyroelectric coefficient. It was found that the pyroelectric coefficient was 115 $\mu C/m^2\ ^oC$. This value was slightly higher than that reported in the literature (Byer and Roundy, 1972). This was probably due to a better quality of material used in this work.

The plots of the polarization versus temperature for the poled PZT and composites having 0.6 and 0.4 volume fraction of PZT were shown in Figure 4.12 to Figure 4.14 respectively. From the slope of these plots, the pyroelectric coefficient for poled PZT and the composites having 0.6 and 0.4 volume fraction of PZT were found to be 74, 54 and 44 $\mu C/m^2\ ^oC$, respectively. It was found that the pyroelectric coefficients of the composites increase with the increase of the volume fraction of PZT. It is assumed that the pyroelectric coefficient arises from two possible factors, electric charges injected from electrodes during poling process, and an electric dipole contribution. The larger contribution due to piezoelectric (secondary pyroelectric effect). Based on these results, it is apparent that the composites consisting of PZT and epoxy in 1-3 connectivity can be used as a pyroelectric detector.

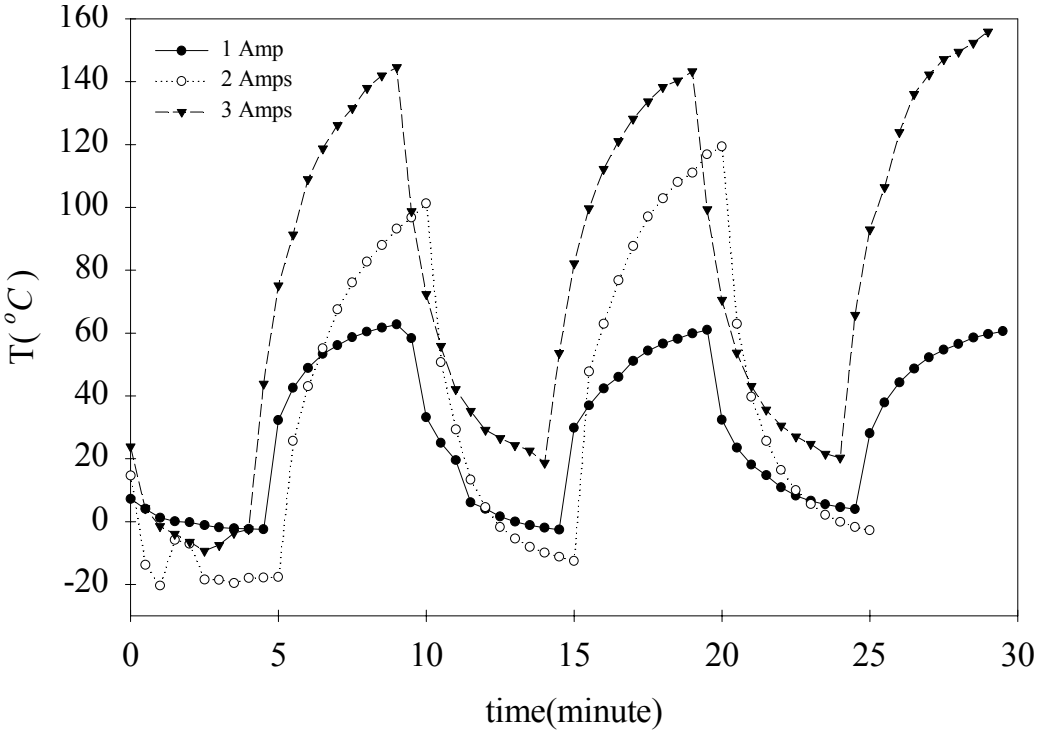

Figure 4.11 A typical temperature patterns used for measuring the pyroelectric coefficient

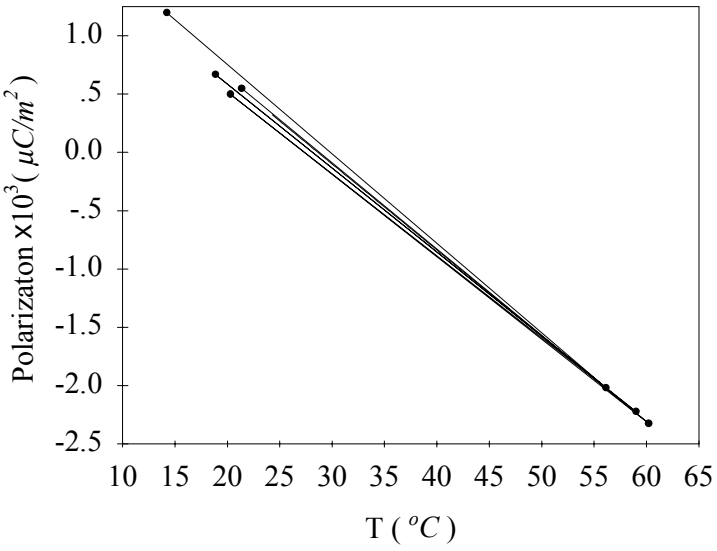

Figure 4.12 Variation of polarization with temperature for the poled PZT(ϕ=1)

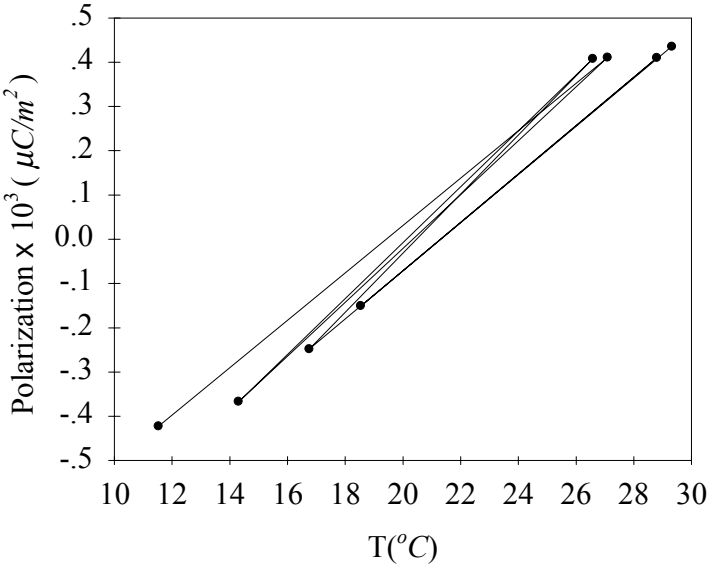

Figure 4.13 Variation of polarization with temperature for 1-3 composite PZT/epoxy (ϕ=0.6)

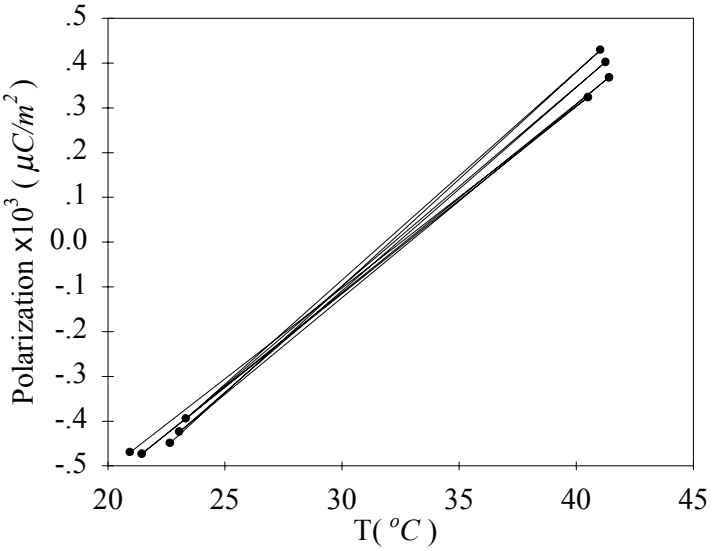

Figure 4.14 Variation of polarization with temperature for 1-3 composite PZT/epoxy (ϕ = 0.4)

Since the 0-3 composite PZT/P(VDF-TrFE) need more complicated poling process. It was found that a breakdown occurred during poling process. The pyroelectricity could not be investigated. It was also difficult to make a reflective surface that could reflect the laser beam in the interferometer setup. So the piezoelectric coefficient of this material was therefore not reported in this work.

However, Ng, Chan and Choy reported the piezo- and pyroelectric of this material (Ng, Chan and Choy, 2000).

3. Evaluation of the thermal diffusivity

As described in chapter 2, thermal diffusivity of the material can be obtained by the phase retardation of the temperature waves passing through that material. In practice, the phase retardation is determined from the pyroelectric current of the detector. In this work the thermal diffusivity measurements were made on the 1-3 composite in both volume fraction of ceramic, epoxy and 0-3 composite PZT/P(VDF-TrFE)

The phase retardation of the temperature waves of the 1-3 composite having 0.4 volume fraction of ceramic in frequency range from 1 *Hz* to 600 *Hz* is shown in Figure 4.15. It is seen from Figure 4.18 that at high frequency, the penetration depth of the temperature waves will becomes very small corresponded to equation (2.62). So, the experimental were made in low frequency range in order that the temperature waves is distributed uniformly across samples thickness. An illustration of the calculation attenuation and phase retardation of the temperature waves for the 1-3 composite with 0.4 volume fraction of PZT is shown in Figure 4.16

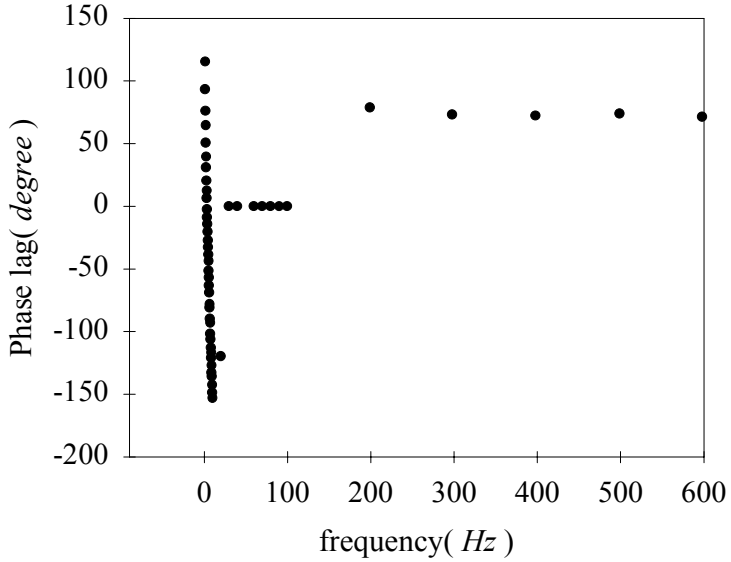

Figure 4.15 The phase retardation of a temperature waves passing through the 1-3 composite PZT/epoxy (ϕ = 0.4) plotted as a function of the modulated frequency.

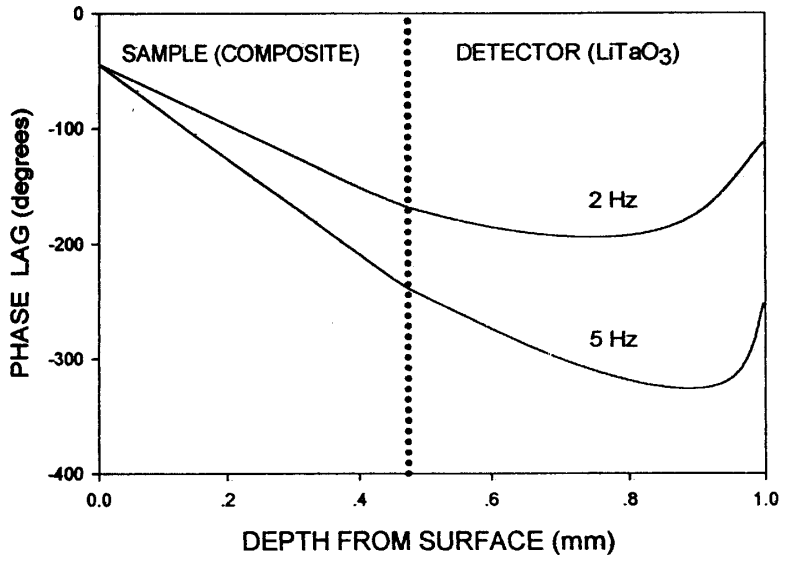

Figure 4.16 An illustration of the calculation attenuation and phase retardation of the temperature waves for the 1-3 composite PZT/epoxy ($\phi = 0.4$)

Experimental phase retardation and pyroelectric current data obtained from 1-3 composite PZT/epoxy having 0.4 and 0.6 volume fraction of ceramic and epoxy in frequency range used for thermal diffusivity data analysis are shown in figure 4.17 to figure 4.22, respectively. It is seen from the figures that the pyroelectric current from the detector are exponentially decay with increasing modulation frequency while the phase retardation of the temperature waves give the 3rd-degree polynomial relation with the modulation frequency.

The unknown thermal diffusivity of the sample was found by fitting the experimental frequency vs phase lag data to the theory by a nonlinear regression algorithm using the mathematics program *Mathematica*. The values of the thermal diffusivity were found to be $2.24\times10^{-7}\, m^2/s$ and $1.43\times10^{-7}\, m^2/s$ for the 1-3 composite PZT/epoxy having 0.4 and 0.6 volume fraction of ceramic respectively and $2.5\times10^{-8}\, m^2/s$ for epoxy.

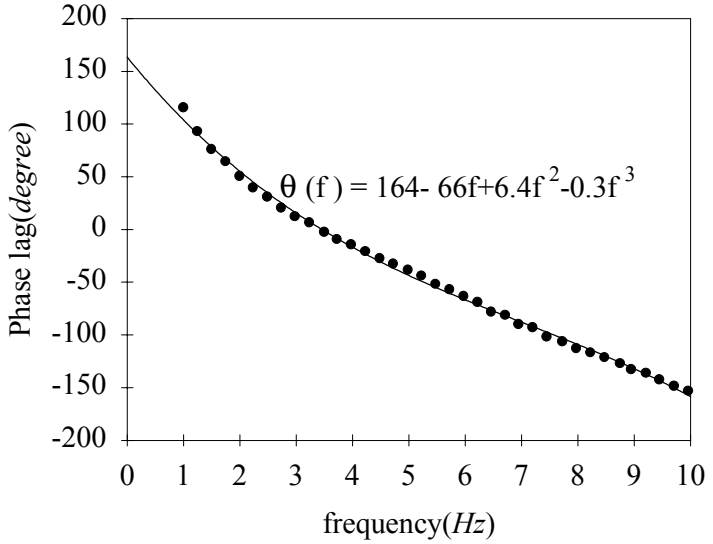

Figure 4.17 The phase retardation of a temperature waves passing through the 1-3 composite PZT/epoxy (ϕ = 0.4) plotted as a function of the modulated frequency.

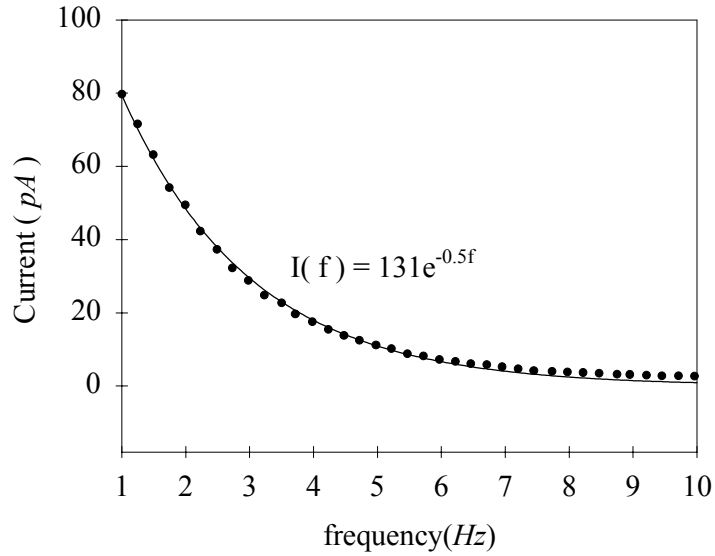

Figure 4.18 Measured current as a function of the modulated frequency for 1-3 composite PZT/epoxy (ϕ = 0.4)

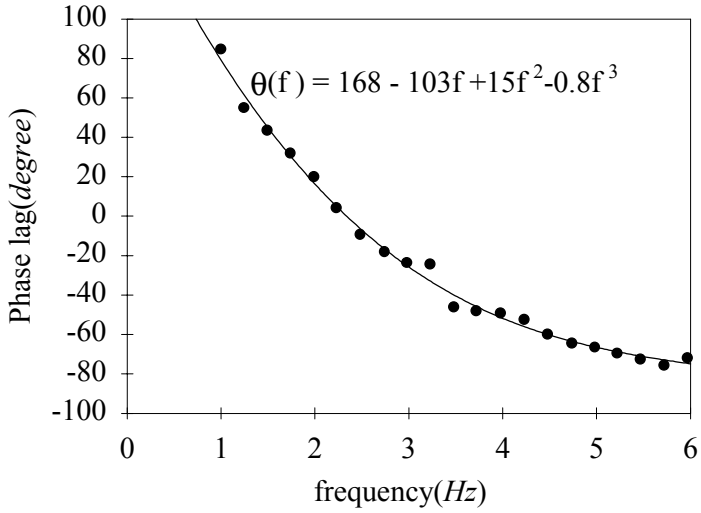

Figure 4.19 The phase retardation of a temperature waves passing through the 1-3 composite PZT/epoxy (ϕ = 0.6) plotted as a function of the modulated frequency.

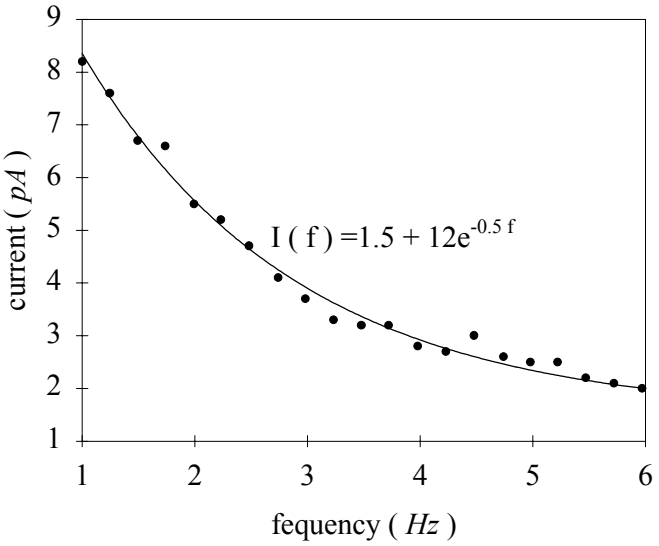

Figure 4.20 Measured current as a function of the modulated frequency for 1-3 composite PZT/epoxy (ϕ = 0.6)

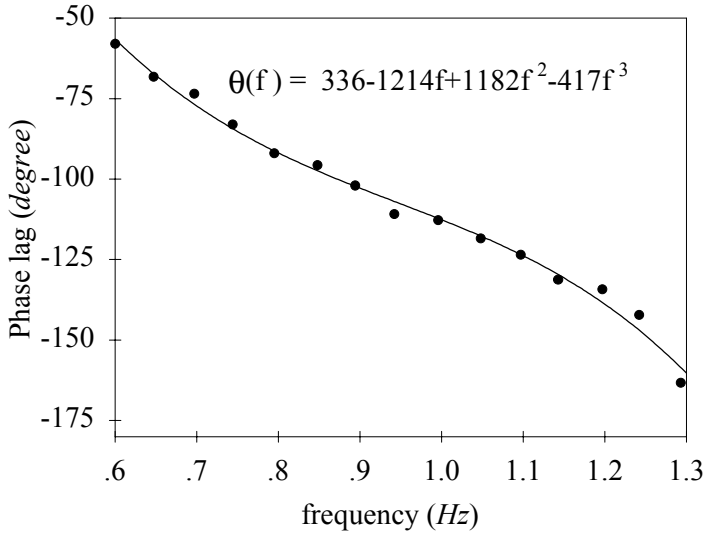

Figure 4.21 The phase retardation of a temperature waves passing through the epoxy plotted as a function of the modulated frequency.

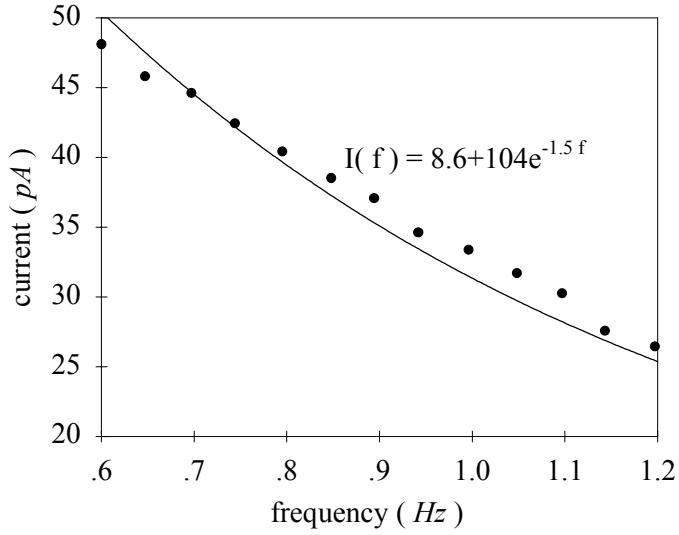

Figure 4.22 Measured current as a function of the modulated frequency for epoxy

The phase retardation obtained from 0-3 composite PZT/P(VDF-TrFE) are shown in Figure 4.23. At low frequency range, this figure indicates that the attenuation and phase retardation of the temperature waves diffused through the thin sample are very small because the sample is very thin. Thus, the appropriate frequency range for thin sample is more than thick sample. For this sample, the appropriate frequency

range is 20 Hz to 300 Hz. The values of the thermal diffusivity of the 0-3 composite were found to be $2.04\times10^{-8}\ \mathrm{m}^2/s$.

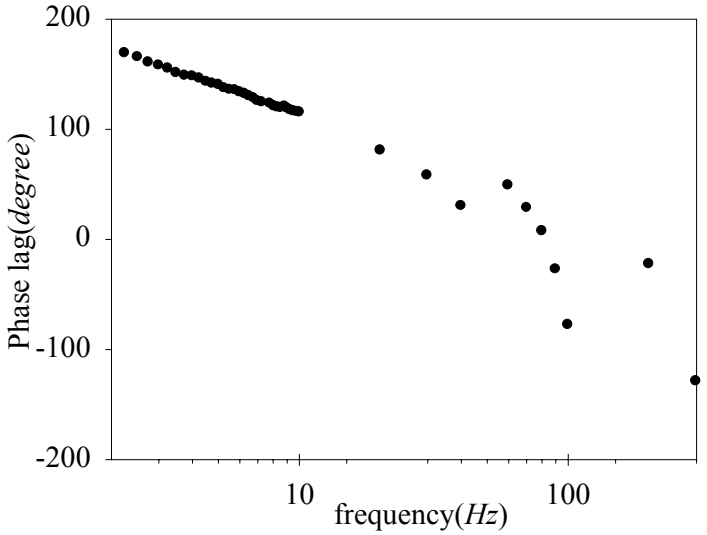

Figure 4.23 The phase retardation of a temperature waves passing through the 0-3 composite PZT/P(VDF-TrFE) (ϕ = 0.3) plotted as a function of the modulated frequency.

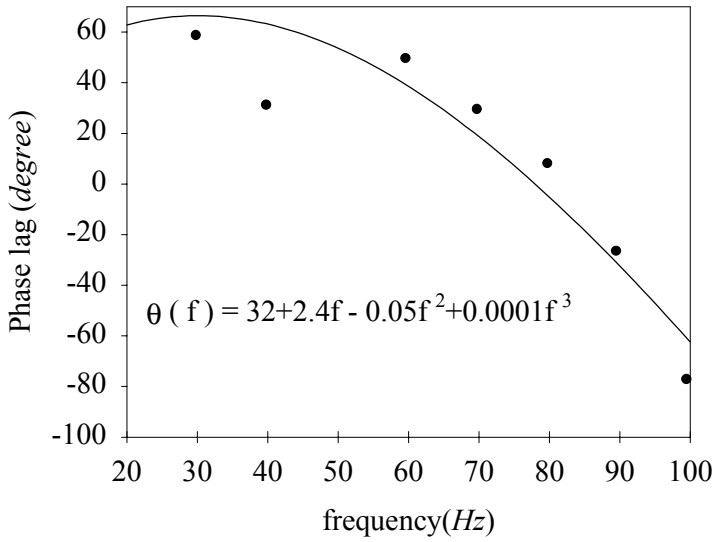

Figure 4.24 The phase retardation of a temperature waves passing through the 0-3 composite PZT/P(VDF-TrFE) (ϕ = 0.3) plotted as a function of the modulated frequency.

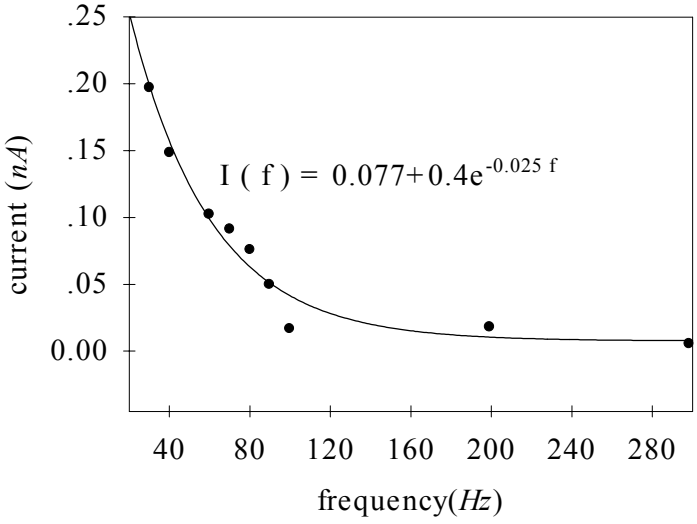

Figure 4.25 Measured current as a function of the modulated frequency for 0-3 composite PZT/P(VDF-TrFE) ($\phi = 0.3$)

4. Application

As mentioned in chapter 2, material properties of the composites relevant to their application in pyroelectric detectors. In a finally part of this work, the 1-3 composite PZT/epoxy having 0.4 volume fraction of ceramic is used as the pyroelectric detector for determining the thermal diffusivity of the $LiTaO_3$. The phase retardation of the temperature waves passing through $LiTaO_3$ is shown in figure 4.26. Figure 4.27 shows the pyroelectric current generating from the composite detector as a result of the temperature waves passing through the $LiTaO_3$ sample plotted against the frequency. The thermal diffusivity if the LiTaO3 was found to be $4.39\times10^{-7}\ \mathrm{m}^2/s$ which was 38% different from the reported value in the literature (Muensit and Lang, in press). This was probably due to heat generated in the epoxy. It was also observed that the composites were mechanically flexible. The relative high piezoelectric and pyroelectric combined with the flexibility suggest that the materials show good promise for applications as piezoelectric transducers and pyroelectric detectors. However, it is important that the structure designs of the transducers or detectors made from the composites take into account the dissipation of the heat generated by either an AC field or sharp temperature changes.

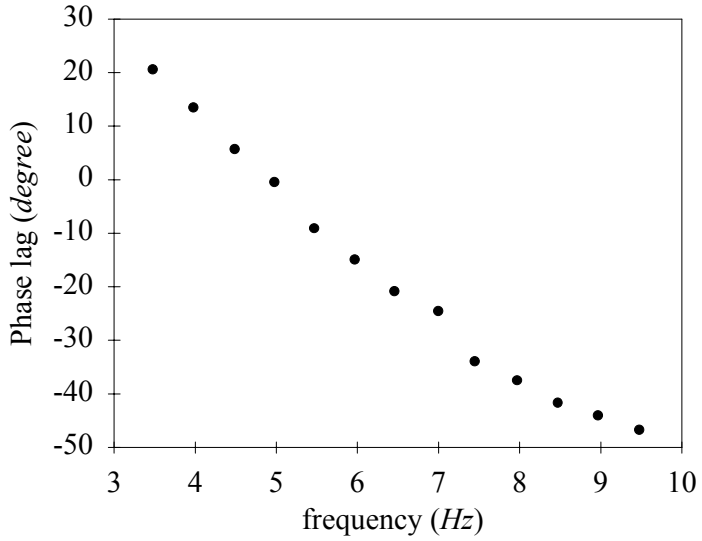

Figure 4.26 The phase retardation of a temperature waves passing through the $LiTaO_3$ plotted as a function of the modulated frequency.

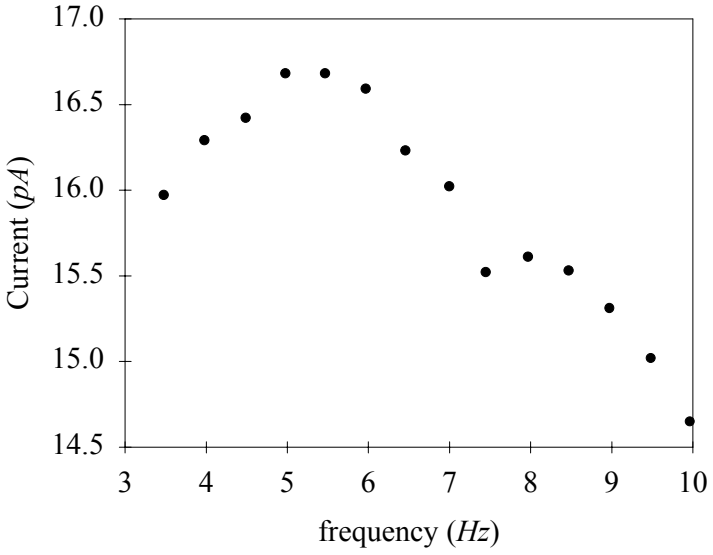

Figure 4.27 Measured current as a function of the modulated frequency for $LiTaO_3$